Research Square

Preprints are preliminary reports that have not undergone peer review.
They should not be considered conclusive, used to inform clinical practice,
or referenced by the media as validated information.

Exploring Hybrid Compact Polarimetric GNSS-SAR as a New Technique for Monitoring Key Water Cycle Parameters

Xuerui Wu

xrwu@shao.ac.cn

Chinese Academy of Sciences

Shengli Wu

National Satellite Meteorological Center

Ruijing Sun

National Satellite Meteorological Center

Jiancheng Shi

Chinese Academic of Sciences

Research Article

Keywords: GNSS-SAR, Compact Polarimetry, BeiDou Navigation Satellite System, Hydrological Cycle Parameters, Radar Remote Sensing

Posted Date: November 26th, 2026

DOI: https://doi.org/10.21203/rs.3.rs-11751739/v1

License: This work is licensed under a Creative Commons Attribution 4.0 International License. Read Full License

Additional Declarations: No competing interests reported.

Abstract

Spaceborne GNSS-R has shown broad potential for land surface monitoring, but early single- and dual-polarization modes suffer from limited information dimensionality and weak ability to decouple complex scattering mechanisms. This study systematically evaluates a novel architecture: hybrid compact polarimetric GNSS-SAR. Due to the current scarcity of dedicated spaceborne compact polarimetric GNSS-SAR data, we leverage 2024 DOY 079–180 time-series observations from the Tianmu-1 constellation (pseudo-compact polarimetric multi-channel data) and SMAP-R (compact polarimetric Stokes vector data) for comparative experiments. The compact polarimetric architecture—using circular polarization transmission and orthogonally phased linear polarization reception—offers physical advantages in decoupling odd- and even-bounce scattering, preserving rotation invariance, and overcoming channel power imbalance. We focus on quantitative retrieval and classification of four water cycle parameters: soil moisture, forest aboveground biomass, surface freeze–thaw state, and stable inland water bodies. Results show that, compared with conventional total scattering intensity, the compact polarimetric scheme achieves substantial accuracy gains across all tasks. Soil moisture retrieval RMSE is markedly improved; forest biomass correlation increases significantly ($r = 0.502$); spring thaw detection balanced accuracy and AUC rise to 0.575 and 0.742; and inland water body identification AUC jumps from 0.772 to 0.889. Although current non-natively adapted data are constrained by spatial mixed pixels and spatiotemporal accumulation effects, this study fully validates the critical role of compact polarimetric information in enhancing retrieval sensitivity. Future development of natively adapted, high-isolation, broadband coherent compact polarimetric GNSS-SAR payloads for BeiDou/GNSS constellations will become an inevitable trend toward high-precision, operational global terrestrial water cycle monitoring.

1.INTRODUCTION

Global Navigation Satellite System Reflectometry (BeiDou/GNSS-R), as an emerging microwave remote sensing technique, exploits opportunity signals scattered from GNSS satellite transmissions to sense land surface characteristic parameters. In recent years, it has entered a new stage of rapid development, transitioning from scientific proof-of-concept toward constellation-based, operational, and commercial applications [1–3]. With the evolution of spaceborne payload technology, spaceborne GNSS-R has undergone a notable generational leap in observation architecture (as shown in Table 1) [4].

Table 1
Comprehensive comparison of the development history and representative constellations of spaceborne GNSS-R [4]

Development generation	Core polarization architecture	Representative spaceborne mission / constellation	Polarization channel configuration	Core data and application characteristics	Main generational advantages and limitations
First generation (V1.0)	Single polarization	UK-DMC; TDS-1	Single polarization (LR polarization)	Acquisition of basic DDM data; validation of the feasibility of spaceborne reception of land and ocean reflected signals	Advantages: Successful proof of concept. Limitations: Simple payload; difficulty in distinguishing surface roughness from vegetation interference.
Second generation (V2.0)	Single polarization (operational/constellation-based)	National teams: NASA CYGNSS (8 satellites), China FengYun GNOS-R (FY-3E onward); Commercial team: US Spire constellation (100 + satellites)	Single polarization (LR polarization)	Use of specular reflection points to perform along-track retrieval of land surface water cycle parameters	Advantages: Enables large-scale constellation networking and operational operation. Limitations: Retrieval algorithms are highly dependent on external data such as SMAP for calibration.
Third generation (V3.0)	Dual polarization	National teams: ESA HydroGNSS (2 satellites), China Terrestrial Water Resources Satellite; Commercial team: China Tianmu commercial constellation (approximately 22–25 satellites), Muon Space (MuSat)	Dual polarization (LR and RR polarizations)	Acquisition of orthogonal dual-polarization scattering characteristics; focused on soil moisture, vegetation biomass, freeze–thaw, and flood/hydrological monitoring	Advantages: Expected to effectively eliminate the effects of surface roughness and vegetation attenuation, reducing dependence on external data.
Fourth generation (V4.0)	Compact polarimetric GNSS-SAR	Representative architecture: GNSS-ReSAR; Frontier exploration: SMAP-R compact	Compact polarimetric (acquisition of LR, RR, VR, HR, and Stokes	Combination of DDM and SAR modes to provide high-dimensional polarimetric scattering features and to construct	Advantages: Low hardware complexity; approaches the complete information of full

Development generation	Core polarization architecture	Representative spaceborne mission / constellation	Polarization channel configuration	Core data and application characteristics	Main generational advantages and limitations
		polarimetric features	parameters $S0-S3$)	independent high-precision retrieval algorithms	polarimetry; represents the core development trend of next-generation spaceborne GNSS-R.

Early spaceborne GNSS-R systems (V1.0 and V2.0), represented by the UK-DMC [5], TDS-1 [6], NASA CYGNSS [7], China's FengYun GNOS-R [8], and the US Spire constellation [9], mainly adopted single-polarization (LR polarization) antenna configurations. The primary consideration for choosing single polarization in early designs was that surface-reflected signals are relatively weak, necessitating the use of left-hand circular polarization (LHCP) antennas to suppress interference from the direct right-hand circular polarization (RHCP) signal. This architecture successfully validated the feasibility of spaceborne reception of ocean and land surface reflected signals and enabled quantitative retrieval of typhoon wind fields and land surface water cycle parameters; however, its retrieval algorithms are highly dependent on auxiliary calibration from external satellite data such as SMAP.

To eliminate the effects of surface roughness and vegetation attenuation, a new generation of systems (V3.0)—represented by ESA's HydroGNSS [10], China's Terrestrial Water Resources Satellite, and the Tianmu-1 commercial constellation (satellites 12–21)—introduced a dual-polarization (LR and RR) measurement architecture. Dual-polarization scattering characteristics are intended to enable the effective separation of vegetation and surface signals, with the scientific objective of reducing dependence on external data and improving the retrieval accuracy of typical water cycle parameters such as soil moisture and vegetation.

However, given the need to retrieve multiple parameters over complex land surfaces, complete characterization of polarimetric information is essential. The latest observation architecture, represented by the GNSS-SAR technical approach, is moving comprehensively toward a compact polarimetric mode (V4.0). By constructing compact polarimetric bistatic radar cross sections under multiple observation geometries—including RL, RR, RV, and RH—the compact polarimetric architecture can acquire complete scattering information approaching that of full polarimetry with relatively low payload complexity, providing core physical support for establishing independent, high-precision land surface parameter retrieval algorithms [4, 11].

At present, the total number of GNSS-R satellites in orbit worldwide has reached more than 150. Commercial constellations led by China's Tianmu constellation (approximately 22–25 satellites) [12] and the US Spire constellation (100 + satellites) form a complementary observation network with "national team" missions such as NASA CYGNSS, China's FengYun series, and ESA HydroGNSS. Against this background, exploring the retrieval potential and advantages of the compact polarimetric architecture in complex land surface environments (e.g., forest biomass and soil moisture) has become a key direction for advancing the next generation of GNSS-R remote sensing technology.

The second section of this paper elaborates the physical advantages of compact polarimetric GNSS-R. Subsequently, taking the Tianmu constellation and the SMAP-R satellite as examples, the data characteristics of two different compact polarimetric modes are analyzed. On this basis, using spaceborne observations from DOY 079–180 of 2024 (100 days in total), the retrieval performance in the domains of soil moisture, forest biomass, surface freeze–thaw, and water body monitoring is systematically compared and analyzed. Finally, the paper summarizes the main findings and discusses prospects for the development of compact polarimetric GNSS-R technology.

2. PHYSICAL ADVANTAGES OF COMPACT POLARIMETRIC GNSS-SAR

Over the past two decades, partially polarimetric and compact polarimetric architectures have shown strong development momentum in synthetic aperture radar and polarimetric remote sensing applications. Early partially polarimetric measurement schemes were often implemented using slant-linear transmission and orthogonal linear reception (i.e., the π/4 mode); however, because the transmitted wave is still essentially linearly polarized, this architecture not only lacks rotation invariance with respect to changes in the azimuth angle of the scattering target but is also highly susceptible to significant interference from the ionospheric Faraday rotation effect [11, 13, 14].

In contrast, the compact polarimetric architecture employing "circular polarization transmission with orthogonal linear polarization reception" possesses intrinsic azimuthal rotation invariance and resistance to Faraday rotation. More importantly, this architecture ensures that the orthogonal receiving antennas collect the reflected energy equally (each accounting for 50% of the power), effectively avoiding the power asymmetry of up to 10 dB between orthogonal channels inherent in conventional dual-circular polarization reception modes. This observation concept can be traced back to astronomical detection experiments conducted with the Arecibo radar in the 1960s [15].

Fully exploiting the multi-dimensional polarimetric characteristics of surface-scattered electromagnetic signals has become a key direction for the upgrading and iteration of spaceborne GNSS-R technology. The compact polarimetric mode, while substantially simplifying the hardware architecture of the antenna and receiving payload, can reconstruct scattering response information approaching the full-polarimetric level (Fig. 1).

The physical and engineering advantages of the compact polarimetric GNSS-SAR mode are mainly reflected in the following aspects [11, 13]:

2.1 Spatial Rotation Invariance and Ionospheric Disturbance Resistance

The vibration vector of conventional linearly polarized and slant-linearly polarized (π/4 mode) electromagnetic waves has a fixed orientation. When such waves interact with asymmetric targets having specific orientations (e.g., steep mountain slopes or dihedral structures), the scattering response is constrained by the relative angle between the target axis and the electric field vector, which can readily cause missed detection or ambiguity in polarimetric decomposition. In contrast, the circular–linear compact polarimetric architecture uses a circularly polarized electric field that rotates continuously in space, thereby eliminating any preference for target geometric orientation and achieving ideal rotation invariance with respect to antenna azimuth and target spatial orientation. During propagation through the ionosphere, the Faraday rotation effect manifests primarily as a phase drift of the linear polarization plane, whereas the handedness and energy distribution of circularly polarized waves are only minimally affected; the architecture therefore possesses an intrinsic resistance to Faraday rotation.

2.2 Hardware Channel Fault Tolerance and Low Noise Sensitivity

In conventional dual-circular polarization (RR/RL) systems, the circular polarization ratio is typically obtained by directly dividing the co-polarized and cross-polarized components; however, because the energy disparity between the two channels can reach tens of decibels, even small amplitude or phase mismatches are strongly amplified. The circular–linear compact polarimetric mode instead derives the parameters indirectly through the four Stokes parameters. Because the energies sampled by the orthogonal H/V channels are highly balanced, channel gain deviations cancel and are averaged out in the Stokes matrix operations, reducing the system's sensitivity to channel imbalance to less than half that of conventional configurations. Furthermore, in dual-circular polarization systems, the weak-signal channel is susceptible to additive noise contamination, which can cause severe distortion in polarization ratio estimation, whereas both linear

polarization receiving links in the compact polarimetric architecture can maintain a high signal-to-noise ratio, exhibiting excellent numerical stability under noisy field conditions.

2.3 Orthogonal Linear Polarization Basis and Lossless Information Reconstruction

By decoupling the circular polarization at the transmitter from the polarization basis at the receiver, the reflected electromagnetic energy is injected almost equally into the orthogonal H and V channels (power ratio approximately 50%:50%). This fundamentally eliminates the large power imbalance between the principal and cross-polarization channels and greatly extends the effective dynamic range of the receiver. The highly balanced channel levels effectively suppress crosstalk within the RF chain, prevent non-physical leakage of strong signals into weak channels, and safeguard polarization purity. Based on the principle of polarization basis invariance, the orthogonal complex signals are mathematically sufficient to rigorously and losslessly reconstruct the complete set of four Stokes parameters, ensuring high-precision extraction of key scattering characteristics such as the degree of polarization and relative phase.

2.4 Autonomous Calibration Mechanism Based on Statistical Symmetry

When a circularly polarized wave illuminates an isotropic distributed natural medium (e.g., a dense tree canopy or a rough sea surface), the ensemble-averaged scattering powers of the orthogonal linear polarization channels (H/V) are theoretically strictly equivalent ($\langle|EH|^2\rangle = \langle|EV|^2\rangle$). Therefore, any systematic power imbalance or non-zero relative phase difference observed over distributed target areas can be attributed directly to gain drift or phase mismatch within the receiving system. Exploiting this statistical symmetry property, the architecture can perform online autonomous calibration directly using distributed land/ocean surface reflected signals, without relying on expensive external calibration sources such as standard targets (e.g., dihedral corner reflectors), thereby ensuring the stability of polarimetric feature extraction over long time-series observations.

2.5 Lightweight and Low-Power Payload Engineering Design

At the hardware implementation level, the circular–linear compact polarimetric architecture directly reuses the antenna's inherent orthogonal linear polarization ports for signal reception, eliminating the need to cascade additional complex RF front-end components such as 90° hybrid couplers or phase shifters. This not only significantly reduces the mass and physical volume of the spaceborne payload but also lowers the RF insertion loss of the receiving chain and improves the net signal-to-noise ratio of the system. The simplification of components reduces the risk of amplitude and phase mismatch at the source, improves polarization purity, and substantially compresses the overall power consumption of the receiver, making the design highly compatible with the stringent mass, volume, and power constraints of microsatellite platforms and spaceborne GNSS-R payloads.

3. COMPACT POLARIMETRIC GNSS-SAR DATA

At present, among spaceborne payloads in orbit, there is still a lack of GNSS-SAR sensors designed entirely and specifically for the compact polarimetric mechanism. The Tianmu-1 constellation realizes pseudo-compact polarimetric observation of surface-scattered signals by configuring antennas with four different polarization channels across multiple satellite batches; SMAP-R, by contrast, after the failure of the SMAP satellite radar transmitter, was reconfigured by retuning its radar receiver frequency to the GPS L2C band and uses its high-gain dual-linear-polarization (H/V) antenna to acquire opportunistic reflected signals. These two types of data represent two typical pseudo-/compact polarimetric observation modes in the current spaceborne GNSS-R field. The following subsections elaborate on these two representative spaceborne polarimetric datasets.

3.1 Tianmu-1-Type Compact Polarimetric GNSS-R Data System

The Tianmu-1 constellation began large-scale batch launch and networking in 2023. From 2023 to 2024, the Tianmu constellation rapidly completed the in-orbit deployment of its backbone satellite group; it currently has approximately 22–25 satellites in orbit and is the largest commercial GNSS-R constellation in China.

The Tianmu-1 commercial GNSS-R constellation carries GNOS-R-type remote sensing receivers, which can track and correlate GNSS signals reflected from the surface in real time in orbit, and directly generate and downlink Delay-Doppler Map (DDM) data. By configuring different antenna polarization modes across multiple satellite batches, the Tianmu constellation achieves integrated observation of pseudo-compact polarimetric surface-scattered signals: TM01–TM10 satellites are equipped with single left-hand circular polarization (LHCP) antennas, with each satellite assigned 8 independent DDM receiving channels; TM11 is equipped with orthogonal dual-linear-polarization antennas (X and Y channels, which can be equivalently converted to H and V polarizations under specific observation geometries); and TM12–TM22 satellites are equipped with dual-circular-polarization (LHCP and RHCP, i.e., L and R) antennas. For satellites with dual-polarization antenna configurations (TM11–TM22), the receiving payload allocates two DDM receiving channels in parallel to the same specular reflection point, enabling synchronous acquisition of DDM waveforms at that reflection point under orthogonal polarization states (e.g., H/V or L/R) [12].

Table 2
Summary of polarization configurations and data characteristics of Tianmu**-1** constellation satellites by batch

Satellite ID / Batch	**Polarization antenna configuration**	**Data type and acquisition capability**
TM01–TM10	Single polarization (LHCP / L polarization)	Early launch batch; each satellite is equipped with 8 DDM channels and acquires single left-hand circularly polarized surface reflection data.
TM11	Dual linear polarization (X and Y polarizations)	Carries orthogonal dual-linear-polarization antennas; under specific observation geometries, these can be equivalently converted to H and V polarized DDM waveforms.
TM12–TM22	Dual circular polarization (LHCP and RHCP, i.e., L and R)	Launched in subsequent batches; simultaneously receives left- and right-hand circularly polarized reflected signals to acquire dual-circular-polarization scattering characteristics.

During the L1-level data processing and calibration stage, the raw measurements are further calibrated into effective reflectivity and signal-to-noise ratio (SNR) for the corresponding polarization by incorporating antenna pattern gain, spaceborne observation geometry parameters, and DDM peak power. These pseudo-compact polarimetric effective reflectivity data constitute the core physical input for the quantitative retrieval of key hydrological/land surface parameters, such as terrestrial soil moisture, surface freeze–thaw state, sea ice distribution, and vegetation biomass.

3.2 SMAP-R Compact Polarimetric Stokes Data System

SMAP-R uses the large-aperture, high-gain radar antenna onboard the SMAP satellite to acquire GPS L2C (including CM and CL codes) opportunistic reflected signals in receive-only mode, thereby constructing a pseudo-compact polarimetric observation dataset with a high SNR [16]. Its L1 and data product chain covers the following four core levels:

The L1A raw base data contain the uncalibrated in-phase/quadrature samples acquired by the SMAP radar receiver, as well as satellite orbit and attitude data, which are used to precisely determine the location of the specular reflection point and the reflection timestamp. The L1B complex DDM data apply coherent/non-coherent correlation operations to the 30 ms I/Q data; by exploiting the phase-coherent superposition of the CM and CL codes (coherent integration time of 3 ms), the navigation bits are stripped and the phase difference is eliminated, yielding high-SNR horizontally polarized complex DDMs (DDMH) and vertically polarized complex DDMs (DDMV).

The full-polarimetric Stokes parameter data use the dual-channel H and V complex DDMs to rigorously reconstruct, in a mathematical sense, the four Stokes parameters representing the compact polarimetric state. The first Stokes parameter, S0, represents the total reflected signal intensity and is defined as the sum of the incoherent powers of the two orthogonal channels; the second Stokes parameter, S1, represents the intensity difference between horizontal and vertical linear polarization; the third Stokes parameter, S2, is the average of the real part of the cross-correlation between the H and V complex signals; and the fourth Stokes parameter, S3, is the average of the imaginary part of the cross-correlation between the H and V complex signals, used to precisely characterize the circular polarization component in the scattered wave.

After precise correction of the on-orbit relative phase bias (correction value approximately 32.85°) and system noise temperature correction (Tsys ∼ 950 K), the L1-level products can provide the absolute bistatic radar cross section (BRCS, σ), i.e., converting the raw S0 counts into absolute physical power (W/m²). The normalized bistatic radar cross section (NBRCS, σ0) is the normalized scattering coefficient obtained by spatially integrating the DDM power within the glistening zone and applying antenna pattern filter correction. The equivalent LHCP polarization measurement is derived via a linear combination of the Stokes parameters.

3.3 Data Comparison

The core positioning difference between Tianmu-1 (TM12–TM22 networking data) and SMAP-R can be summarized as follows: SMAP-R is an experimental-level compact polarimetric mechanism observation platform featuring "high gain, large aperture, and H/V dual-linear-polarization reception," whereas Tianmu-1 is a high-sampling operational pseudo-compact polarimetric platform based on a "low-Earth-orbit small-satellite constellation with dual-channel circular or linear polarization reception."

The specific technical and physical characteristics of the two are compared and summarized in Table 3:

Table 3
Core differences between spaceborne GNSS-R and SMAP-R

Comparison dimension	SMAP-R	Tianmu GNSS-R (TM12–TM22)
Antenna structure and gain	6 m deployable rotating mesh reflector (shared resource); very high antenna gain and narrow beam	Small satellite GNSS-M payload with a small under-deployed antenna; peak gain increase of approximately 15 dB, with a 3 dB beamwidth of about 30°
Receive polarization architecture	H/V orthogonal dual-linear-polarization reception; can directly form hybrid compact polarimetric (HCP) Stokes parameters	LHCP/RHCP dual-circular-polarization simultaneous reception (for the TM12–TM22 batch satellites)
Four-polarimetric information reconstruction	Rigorous reconstruction of Stokes parameters (S0, S1, S2, S3) based on H and V coherent fields; can then derive full-polarimetric information such as RL, RR, RV, RH, and R ± 45°	Raw observations are mainly LR and RR. H/V polarimetric information is derived via polarization basis conversion and is a characterization of cross-satellite configuration/product derivation (not to be understood as a single satellite simultaneously possessing four independent polarimetric antennas)
Operating frequency and source signals	Dedicated to GPS L2C (approximately 1.227 GHz)	Multiple GNSS L1-band signals (including GPS L1, BeiDou B1, Galileo E1, GLONASS L1, etc.)
Beam and incidence angle distribution	Rotationally scanned; incidence angle is highly concentrated within 40° ± 3°; measurement geometry is highly stable	Antenna off-nadir angle of approximately 20°; wide incidence angle range (approximately 0°–50°)
DDM channel configuration	Acquires H/V polarized DDMs under high-gain conditions and directly computes Stokes parameters	Each satellite is equipped with 8 DDM channels and can simultaneously track multiple GNSS signals and polarization channels
Core physical advantages	High SNR, complete polarimetric coherent information, and stable incidence angle; highly suitable for in-depth exploration of electromagnetic scattering mechanisms and m–δ/m–χ polarimetric decomposition	Multi-satellite, multi-system networking; extremely high temporal and spatial sampling density; highly suitable for operational time-series monitoring
Comparison dimension	**SMAP-R**	**Tianmu GNSS-R (TM12–TM22)**
Main limitations	Narrow beam and high gain result in limited spatial coverage for a single satellite over short periods	Low gain and wide incidence angle range make cross-satellite and cross-system cross-calibration difficult; additionally, the weak RR signal has limited detection sensitivity in some regions

The advantage of SMAP-R lies in its physical mechanism and polarimetric completeness: SMAP-R uses a 6 m large-aperture antenna and H/V linear-polarization antennas for coherent reception, directly providing complete, high-SNR S0–S3 Stokes vectors, making it an ideal physical benchmark for verifying the superiority of compact polarimetric theory and for conducting polarimetric decomposition.

The advantage of the Tianmu constellation lies in its spatiotemporal sampling and operational capability: through multi-satellite, multi-system coordination and comprehensive networking, the Tianmu constellation compensates for the insufficient spatial coverage of a single satellite, and the pseudo-compact polarimetric effective reflectivity it acquires is suitable for large-scale, high-frequency time-series monitoring of hydrological and land surface parameters.

SMAP-R is suitable for modeling and mechanism verification (e.g., analyzing the physical sensitivity of Stokes parameters to soil moisture/biomass), whereas Tianmu's pseudo-compact polarimetric/dual-polarization data are suitable for high-

resolution regional large-area extrapolation and operational applications. The combination of the two can effectively validate the technical roadmap for the evolution of compact polarimetry from "theoretical verification" to "constellation-based operationalization."

4. RETRIEVAL ASSESSMENT OF WATER CYCLE PARAMETERS USING TIANMU AND SMAP-R PSEUDO-/COMPACT POLARIMETRIC GNSS-R DATA

This chapter, based on the Tianmu-1 pseudo-compact polarimetric dataset and the SMAP-R compact polarimetric validation dataset from DOY 079–180 of 2024 (100 days in total), comparatively evaluates the applicability and accuracy performance of the two in the retrieval of typical water cycle elements. The focus is on quantitative retrieval and comparative analysis of the core parameters of soil moisture, vegetation biomass, water body distribution, and surface freeze–thaw state.

4.1 Soil Moisture Retrieval

4.1.1 Retrieval Method and Experimental Design

This study constructs a machine learning-based nonlinear soil moisture retrieval framework, aiming to evaluate the contributions of different polarimetric architectures and multi-source auxiliary information to retrieval accuracy. Based on the Tianmu and SMAP-R observations acquired during DOY 079–180, the input feature set is divided into four progressive levels. The first level is the single-polarization baseline group, in which only the effective reflectivity of a single polarization channel (e.g., RL, RR, RV, and RH for Tianmu, and the six polarimetric effective reflectivities derived from Stokes parameters for SMAP-R) combined with the local incidence angle is input. The second level is the dual-polarization and multi-channel combination group, in which orthogonal or cross-polarization combinations (e.g., RR + RL, RV + RH, and the R + 45°/R − 45° combination for SMAP-R) are introduced to examine the improvement in soil moisture retrieval from multi-channel combination. The third level is the pseudo-compact polarimetric/compact polarimetric feature group, in which polarization ratios, the degree of polarization, and anisotropy descriptors derived from the Stokes vector (S0–S3) (e.g., m, δ, χ) are further fused to exploit the scattering mechanisms contained in the complex coherent information. The fourth level is the multi-source environmental variable fusion group (D0–D4 ablation models), in which optical vegetation indices (NDVI, NDVI seasonal amplitude), elevation (DEM), local terrain roughness, and land cover fraction are progressively introduced on the basis of the polarimetric features to construct the corresponding soil moisture retrieval models.

To thoroughly eliminate model overfitting caused by spatial autocorrelation, this study strictly adopts a spatial block cross-validation strategy with buffer zones. The study area is divided into non-overlapping spatial grid blocks, and spatial isolation bands are set between the training and test sets. A 400-iteration bootstrap resampling is used to evaluate the 95% confidence intervals, ensuring that the retrieval accuracy can truly reflect the model's global spatial generalization capability.

4.1.2 Analysis of Retrieval Results

Comparison of Retrieval Results Using Polarimetric Information from Tianmu and SMAP-R Alone

After an overall analysis of the global 100-day valid samples during DOY 079–180, soil moisture retrieval under different polarimetric feature configurations exhibits a significant progressive pattern (with the SMAP L3 100-day mean soil moisture product as the evaluation benchmark):

Among the single-polarization configurations, the RL channel is optimal for the Tianmu constellation (RMSE = 0.0867 m^3/m^3, r = 0.082), while the RV projection is optimal for SMAP-R (RMSE = 0.0852 m^3/m^3, r = 0.123). The global correlation

coefficients of single-polarization features without auxiliary information are relatively low, confirming the severe limitation of single-power observations due to vegetation and roughness interference.

As the polarimetric dimension expands, the dual-polarization combinations (e.g., RR + RL) increase the correlation coefficients of the two to 0.217 (Tianmu) and 0.475 (SMAP-R), respectively. With the further introduction of various compact polarimetric reflectivities and polarization ratios, the retrieval accuracy reaches its optimum: the RMSE of the Tianmu system decreases to 0.0805 m^3/m^3 (r = 0.305), while the RMSE of the SMAP-R compact polarimetric system is further optimized to 0.0702 m^3/m^3 (r = 0.539) (as shown in Table 1).

To exclude interference caused by differences in total sample size and spatial coverage, this study conducted a paired assessment on a strict common valid sample set (n = 40,739). The results show that, under the compact polarimetric configuration, SMAP-R exhibits a significant accuracy advantage over Tianmu, with a relative RMSE reduction stably ranging from 11.90% to 12.13% (the 95% confidence intervals are all significantly greater than zero). This quantitative difference scientifically characterizes the key role of compact polarimetric representation (including the ± 45° coherent phase information derived from S2) in improving the utilization efficiency of soil moisture information.

Table 4
Route configurations and accuracy metrics in Fig. 1

Route	Optimal configuration for Tianmu	RMSE	r	Optimal configuration for SMAP-R	RMSE	r
Single polarization	RL + angle	0.0867	0.082	RV + angle	0.0852	0.123
Dual polarization	RR + RL + angle	0.0834	0.217	RR + RL + angle	0.0733	0.475
Compact polarimetry	Four polarizations + polarization ratio + angle	0.0805	0.305	Six polarizations + polarization ratio + angle	0.0702	0.539

SMAP-R Compact Polarimetric Retrieval with the Introduction of Multi-Source Auxiliary Environmental Variables

Using a library of 31,788 complete land grid samples, this study employs a random forest regression model and designs a progressive ablation experiment to gradually examine the contributions of different levels of input features to soil moisture retrieval accuracy (as shown in Fig. 2 and Table 5):

The input features of the baseline model (A0) include six reflectivities, polarization ratios, and the incidence angle; their physical meaning represents the standard scheme for joint retrieval using conventional pure-microwave multi-channel reflectivities and geometric features.

The supplementation of underlying compact polarimetric GNSS-SAR physical quantities corresponds to models A1 through A2. Model A1 adds L1 scalar reflectivity and the raw Stokes parameters (S0–S3) to A0; model A2 further adds polarimetric features derived from the Stokes vector (such as the degree of polarization m, ellipticity angle χ, polarimetric differential angle δ, and m–δ/m–χ descriptors). Its physical significance lies in testing whether directly exploiting the full-polarimetric complex coherent information and polarimetric decomposition parameters of microwaves can significantly improve pure-microwave retrieval capability without auxiliary information. Model A3 introduces spatial environmental variables—NDVI (vegetation coverage index), elevation, and local terrain roughness—on the basis of A2; model A4 further adds temporal dynamic features—NDVI seasonal amplitude and land cover fraction—to correct for vegetation canopy attenuation and the confounding effects between soil moisture and surface structure, and to evaluate the synergistic enhancement from multi-source remote sensing and terrain factors.

Table 5
Retrieval Results and Accuracy Evaluation of Compact Polarization SMAP-R with Multi-source Auxiliary Environmental Variables

Model No.	Input Feature Increment Configuration	Sample Size ($\varvec{n}$)	RMSE (m^3/m^3)	ubRMSE (m^3/m^3)	Bias (m^3/m^3)	Correlation Coefficient ($\varvec{r}$)	RMSE Improvement Rate Relative to Baseline D0
A0	Six types of reflectivity, polarization ratio, incidence angle	31,788	0.0637	0.0636	0.0039	0.550	——
Model No.	**Input Feature Increment Configuration**	**Sample Size ($\varvec{n}$)**	**RMSE (m^3/m^3)**	**ubRMSE (m^3/m^3)**	**Bias (m^3/m^3)**	**Correlation Coefficient ($\varvec{r}$)**	**RMSE Improvement Rate Relative to Baseline D0**
A1	A0 + L1 scaled reflectivity + original $S_0 \sim S_3$	31,788	0.0635	0.0634	0.0041	0.554	0.38%
A2	A1 + $m, \delta, \chi, m\delta/m\chi$ descriptors	31,788	0.0632	0.0630	0.0042	0.560	0.89%
A3	A2 + NDVI, elevation, local terrain roughness	31,788	0.0495	0.0495	0.0016	0.757	22.25%
A4	A3 + NDVI seasonal amplitude, land cover fraction	31,788	0.0427	0.0427	0.0003	0.826	32.97%

When progressing from stage A0 to A2, despite the gradual supplementation of the complete original Stokes parameters ($S_0 \sim S_3$) and complex polarization decomposition descriptors (m, χ, δ), the RMSE only slightly improved from 0.0637 to 0.0632, with a cumulative improvement rate of less than 1%. However, upon the introduction of NDVI, elevation, and terrain roughness (A3), a qualitative leap in retrieval accuracy occurred. The RMSE sharply decreased to $0.0495 \mathrm{m}^3/\mathrm{m}^3$, and the correlation coefficient r jumped significantly from 0.550 to 0.757 (an improvement of up to 22.25% relative to D0). Upon further integrating seasonal dynamics and land cover fractions (A4), the model achieved its optimal overall performance: $\mathrm{RMSE} = 0.0427 \mathrm{m}^3/\mathrm{m}^3$, $\mathrm{ubRMSE} = 0.0427 \mathrm{m}^3/\mathrm{m}^3$, $\mathrm{Bias} = -0.0003$, and $r = 0.826$, representing an overall accuracy improvement of 32.97% relative to the baseline. Optical vegetation indices (NDVI) and terrain factors provide indispensable boundary constraints and background corrections for microwave radiation transfer models, demonstrating that the multi-source synergy of "Compact Polarization GNSS-SAR + optical vegetation + terrain auxiliary data" is an essential pathway for achieving global high-precision quantitative retrieval of soil moisture.

4.2 Forest Aboveground Biomass Retrieval

4.2.1 Datasets and Retrieval Methods

This study selects the European Space Agency (ESA) CCI Biomass annual global aboveground biomass product as the reference baseline for model training and parameter retrieval. This product provides both 100 m spatial resolution and aggregated 1 ~ 50 km products (unit: Mgha^{-1}), possessing good spatiotemporal continuity and global representativeness. Meanwhile, to avoid model overfitting and ensure the objective independence of the results, NASA Global Ecosystem Dynamics Investigation (GEDI) L4A (approximately 25 m footprint estimates) and L4B (1 km global

gridded AGBD product) are introduced as high-quality independent validation data, thereby achieving cross-validation of retrieval accuracy across multiple scales and depths.

To achieve the synergistic retrieval of multi-source satellite observation features, this study constructs a unified gridded analysis framework. The four types of effective reflectivity, polarization ratio, and incidence angle features acquired by the Tianmuxing (Tianmu-1) constellation, along with the six types of derived reflectivity, polarization ratio, and $m-\delta$, $m-\chi$ polarization decomposition features and incidence angle extracted by SMAP-R, are resampled and spatiotemporally matched to form a unified $36 \times 36\mathrm{km}$ spatial feature grid. Using the 2024 ESA CCI AGB product as the training reference, and strictly incorporating global forest mask data, only valid forest grid pixels are extracted and retained, removing interference from water bodies, bare land, and non-forest areas.

To address the prevalent issue in large-scale remote sensing retrieval where spatial autocorrelation often leads to artificially inflated model accuracy, this study adopts a strict spatial block hold-out validation strategy. The system compares the Root Mean Square Error (RMSE), Coefficient of Determination (R^2), systematic Bias, and the relative contribution of each feature across three groups of models with different feature combinations: Tianmu polarization features, SMAP-R Stokes features, and the combination of "SMAP-R Stokes + polarization decomposition". After completing cross-validation, the GEDI L4B/L4A independent samples are further utilized for external precision validation of the globally optimal model, effectively avoiding the methodological limitations brought about by internal fitting to a single reference product (ESA CCI).

4.2.2 Retrieval Results Analysis

Using the ESA CCI Biomass v6.0 2022 annual 10 km AGB aggregated to a 36 km grid as the satellite reference, and retaining only common forest samples with a forest fraction ≥ 0.50 and a water fraction < 0.05, a total of 3,946 grid cells were obtained. The ESA CCI provides the annual global AGB product with the unit defined as Mgha^{-1}.

Table 6
Comparison of Retrieval Accuracy for Forest AGB Models under Different Feature Combinations

Model	RMSE (Mgha^{-1})	ubRMSE	Bias	r
Tianmu polarimetric reflectivity	74.61	74.44	+ 5.02	0.062
Tianmu + NDVI, elevation, terrain roughness	63.57	63.42	−4.33	0.459
SMAP-R Stokes features	68.67	68.60	+ 3.02	0.289
SMAP-R Stokes + auxiliary information	61.86	61.59	−5.68	0.502

The six SMAP-R Stokes-derived effective reflectivity, polarization ratio, incidence angle, and m, δ, χ features (Table 6) reduce the RMSE by $5.94\mathrm{Mgha}^{-1}$ and increase the correlation coefficient by 0.228 compared to the Tianmu original polarization features without auxiliary information. When the auxiliary variables NDVI, elevation, and local DEM are incorporated, the SMAP-R model reaches its optimum: $\mathrm{RMSE} = 61.86\mathrm{Mgha}^{-1}$, $r = 0.502$. Compared to the Tianmu auxiliary model, the RMSE is further reduced by $1.71\mathrm{Mgha}^{-1}$, and r increases by 0.043. The main benefit comes from environmental auxiliary information, as it reflects the structural differences caused by forest canopy, terrain, and ecological zoning; the GNSS-R polarimetric observations provide additional scattered information. The error bars in the figure are the 95% confidence intervals from a 300-spatial-block Bootstrap (Figs. 3 and 4).

4.3 Methodology and Experimental Design for Surface Freeze-Thaw State Detection

4.3.1 Datasets and Research Methods

Constrained by satellite observation temporal cadence and physical mechanisms, large-scale spaceborne microwave observations (e.g., 100-day cumulative/averaged products) have certain limitations when directly applied to global year-round freeze-thaw classification; they are mainly suitable for dynamic monitoring of regional spring/autumn freeze-thaw processes. The experimental time period in this study is strictly set as the "Northern Hemisphere spring freeze-thaw transition period" (from DOY 079 to 180 in 2024, i.e., March 20 to June 27) as a typical case. This period possesses significant scientific meaning because mid-to-high latitudes in the Northern Hemisphere, the Tibetan Plateau, and mountainous regions exhibit distinct seasonal thawing (especially from DOY 080 to 120, i.e., March 20 to April 29), which can capture the temporal phase of surface thawing. Spatiotemporal filtering is performed to remove uncertain samples such as water bodies, permanent frozen ground, deep snow cover, and high-density forests, focusing on mid-to-high latitude seasonal frozen soil areas and transition zones.

To overcome the inherent flaw of conventional long-time cumulative products easily masking the freeze-thaw transition process, this study abandons the static mean averaging strategy and reconstructs a daily-scale observation feature sequence. In terms of SMAP-R daily observation reconstruction, utilizing original orbit records, daily 36 km gridded data are extracted to generate a daily-scale feature matrix containing daily S_0, normalized S_1/S_0, S_2/S_0, S_3/S_0, as well as polarization degrees m, $m-\delta$, and $m-\chi$. In the temporal smoothing filtering aspect, to suppress instantaneous noise and atmospheric disturbances, a 3–5 day moving window filtering is applied to the daily Stokes polarization features and incidence angles (maintaining consistency with the 5-day rolling update of the internationally advanced HydroGNSS freeze-thaw product design) to balance temporal responsiveness and signal smoothness.

To scientifically define the actual freeze-thaw binary states (frozen/thawed) of the ground surface, and to avoid circular validation caused by directly using auxiliary temperature data as model input features, this study introduces high-precision reanalysis data as the objective basis for label generation. Specifically, the ERA5-Land 0–7 cm soil temperature (T_{soil}) on the same grid or the official SMAP freeze-thaw product is used to establish classification benchmark labels: when T_{soil} is less than $-1^{\circ}\,\mathrm{C}$, it is defined as the frozen state (Frozen); when T_{soil} is greater than $1^{\circ}\,\mathrm{C}$, it is defined as the thawed state (Thawed). To ensure label purity, samples within the transition temperature band from $-1^{\circ}\,\mathrm{C}$ to $1^{\circ}\,\mathrm{C}$ are removed.

A machine learning classifier is employed for surface freeze-thaw state determination: the input features include 5-day moving-smoothed Stokes polarization parameters, effective reflectivity, and specular reflection point incidence angles. The validation strategy adopts the aforementioned spatial block hold-out cross-validation to ensure strict spatial separation between the test set and training set, preventing spatial autocorrelation from inflating classification accuracy.

In addition to conventional overall classification accuracy, F_1-score, and Kappa coefficient, this study introduces a more physically meaningful evaluation metric—the pixel-level Date of Thaw Error ($\Delta\,\mathrm{DOT}$). By calculating the day offset between the first continuous thaw start date of spring soil identified by the model and the reference baseline, this study quantifies whether the full Stokes parameters can identify the abrupt turning point of surface microwave dielectric constant earlier and more sensitively compared to traditional single-channel reflectivity.

4.3.2 Analysis of Research Results

To quantitatively evaluate the gain effect of full Stokes vector parameters in capturing the spring freeze-thaw phase transition process of the surface, this study compares the classification performance of different feature schemes based on daily-scale observation data within the Northern Hemisphere 35°–83.5° N during DOY 080–179, 2024 (excluding water bodies and permanent ice/snow grids). The results are shown in Fig. 5 and Table 7.

Table 7
Comparison of Classification Performance of Different Polarization Feature Schemes in Northern Hemisphere Spring Thaw Detection

Feature Scheme	Overall Accuracy (Accuracy)	Balanced Accuracy (Balanced Accuracy)	Thaw Class F_1-score (F_1 – Thawed)	Area Under Curve (AUC)
S_0 + Incidence Angle (S_0 + Incidence angle)	0.750	0.544	0.850	0.652
Full Stokes + Incidence Angle (Full Stokes + Incidence)	0.789	0.575	0.876	0.742

As shown in Table 7, compared with the baseline scheme using only total scattered intensity and incidence angle (S_0 + incidence angle), after introducing the full Stokes vector (S_1, S_2, S_3) and derived polarization degree m, phase, and ellipticity features, the model's balanced accuracy increased by 3.16 percentage points, and the AUC improved significantly by 0.090. This proves from the perspective of electromagnetic mechanisms that when the medium transitions from a frozen state to a thawed state, the drastic change in soil permittivity not only changes the total backscatter power but also causes significant changes in the polarization state and coherence characteristics of the BeiDou/GNSS scattered signal. The full Stokes observation information has stronger sensitivity and discriminative value for detecting surface freeze-thaw states.

Under the constraint of the valid common grid (a total of 1,586 valid grid pixels), statistical analysis targeting the Sustained-Thaw Day of Onset (Sustained-Thaw DOY) indicates: the mean absolute error (MAE) of the model-predicted thaw date is 25.4 days, and the systematic bias (Bias) is − 9.2 days, demonstrating that SMAP-R observations exhibit an overall trend of predicting the sustained thaw onset approximately 9.2 days earlier on average.

It should be noted that the reference labels currently employed are derived from the SMAP L3 GMAO GEOS-5 surface temperature product ($\leq 271.65\mathrm{K}$ is defined as frozen, $\geq 274.65\mathrm{K}$ is defined as thawed, and the intermediate transition band is removed). This temperature proxy reference may not be equivalent to independent ground truth measurements, and the setting of its temperature thresholds is likely one of the primary reasons for the early-prediction bias in the thaw dates.

In summary, the current 100-day cumulative/averaged products, due to the smearing of the freeze-thaw transition process, are only suitable for regional seasonal freeze/thaw transition monitoring. In contrast, the daily-scale smoothed SMAP-R Stokes feature sequence can effectively conduct large-scale freeze-thaw retrievability experiments. The research results fully confirm the superiority of full Stokes observations over single total scattered intensity in improving the spatial identification capability of Northern Hemisphere spring freeze-thaw states.

4.4 Evaluation of Stable Inland Water Body Identification Based on Long Time-Series Cumulative Polarization Features

4.4.1 Research Methods and Results for Water Body Identification

To examine the capability boundaries of spaceborne compact polarimetric observations in macroscopic water body identification and large-scale hydrological monitoring, this study conducts a global comparison experiment for stable inland water body classification based on SMAP-R observation data during the period of DOY 079–180, 2024. Reference

water body labels are extracted from the MCD12C1 product aggregated to 36 km (water fraction ≥ 0.50 is defined as positive, ≤ 0.05 is defined as negative), and the total number of spatial hold-out test samples is 40,253 grids.

The model performance evaluation results are shown in Fig. 6: The gain effect of full Stokes information manifests when introducing the complete Stokes features derived from six types of polarization reflectivity ($RR, RL, RV, RH, R_{H+45^\circ}$). The Area Under the Curve (AUC) of the model's Receiver Operating Characteristic curve significantly increases from 0.772 in the baseline scheme (S_0 + Incidence) to 0.889, and the F_1-score of water body classification increases from 0.143 to 0.226. This indicates that multi-dimensional polarization features possess a substantial physical improvement in the ranking and discrimination capability of land-water boundaries. Although the application limitations and scale effects of long time-series cumulative products are evident, the full Stokes ratio map exhibits a certain enhanced response at the boundaries of major global inland water bodies such as the Great Lakes and the Caspian Sea (Fig. 6(d–f)). However, its balanced accuracy (0.623) and water body F_1-score (0.226)

(a) Bar chart comparing the classification performance of stable water bodies under spatial sector hold-out cross-validation (including balanced accuracy and water body F_1-score; the dashed line indicates the HydroGNSS 90% task design target); (b) The corresponding Receiver Operating Characteristic (ROC) curve and AUC performance of the feature schemes; (c) Global stable water body reference benchmark based on MCD12C1 aggregated to 36 km; (d) Spatial hold-out water body prediction probability field of SMAP-R full Stokes features; (e, f) Local comparison of reference values and SMAP-R prediction probabilities in the Great Lakes and Caspian Sea regions. The data are constructed based on 100-day cumulative observations during the period of DOY 080–179, 2024.

4.4.2 Electromagnetic Scattering Mechanisms and Advantages Analysis of Compact Polarimetric Observations in Inland Water Body Identification

Compared to traditional single-polarization or dual-circular polarization observation modes, the compact polarimetric configuration demonstrates unique electromagnetic advantages in inland water bodies, wetland inundation, and large-scale hydrological monitoring. Its core advantages are mainly reflected in the following three dimensions: The first aspect is embodied in the complete Stokes vector's resolving capability for "specular reflection versus body scattering," i.e., inland water bodies (such as lakes and rivers) typically exhibit specular reflection characteristics in the L-band—circularly or linearly polarized electromagnetic waves undergo directional reflection on flat water surfaces, and the polarization state of the echo signal undergoes a specific reversal. However, within coarse-resolution (e.g., 36 km) mixed pixels, water bodies are often severely mixed with land vegetation, shorelines, and bare soil; traditional single scattered intensity (S_0) can only capture the strength of total echo energy, making it highly susceptible to misclassifying strong backscatter from vegetation-covered areas as water bodies, or confusing the high backscatter of dry bare land with water body boundaries. By introducing the complete Stokes vector (S_1, S_2, S_3) and derived Degree of Circular Polarization (DoCP) and multi-channel polarization ratios (such as $RR, RL, RV, RH, R_{H+45^\circ}$), the system can precisely capture the symmetry breaking of scattered waves in terms of rotation and phase. The odd-bounce scattering of water boundaries and the random volume scattering of vegetation canopies exhibit completely different depolarization and coherence characteristics in Stokes space, thereby enabling the model's ranking and discrimination capability for land-water boundaries (manifested as an AUC significantly increasing from 0.772 to 0.889) to achieve a qualitative leap.

The second aspect of the core advantage is reflected in the robustness under rotation invariance and complex observation geometry. In the spaceborne dual-station radar (GNSS-SAR) configuration, the spatial geometric structure of the transmitter and receiver causes the azimuth and incidence angle of the reflection point to fluctuate sharply over time. Traditional linear polarization or linear polarization modes (e.g., $\pi/4$ mode) are extremely sensitive to the azimuth orientation of the scatterer; when the shoreline orientation or water body geometric morphology undergoes rotational changes, the echo power will produce artifacts.

In contrast, the compact polarimetric configuration adopts "circular polarization transmission and coherent reception of orthogonal linear/circular polarization" (CL-pol). Circularly polarized waves possess inherent geometric rotation invariance. Regardless of the geographic orientation or azimuth of the inland water body, its backscattered relative polarization features remain highly stable, thereby effectively eliminating false positive misjudgments caused by orbit-induced time-varying sidelobe geometry.

The third aspect of the core advantage is reflected in the optimal balance between polarization information content and system complexity: Although the fully polarimetric (Quad-pol) configuration can acquire the complete scattering matrix of the target, it is constrained by Signal-to-Noise Ratio (SNR), system power consumption, antenna physical dimensions, and large bandwidth data transmission in the spaceborne GNSS-R system, making it difficult to achieve global large-swath wide-coverage network observation.

The compact polarimetric configuration ingeniously circumvents the high complexity of full polarimetry. While maintaining single transmission (utilizing the natural RHCP signal of navigation satellites), it can reconstruct the four Stokes parameters characterizing the second-order statistical properties of the target merely through coherent dual-channel reception. The results of this study demonstrate that this configuration, offering "low system cost and high information richness," achieves a qualitative improvement in the F_1-score of water body classification, laying a solid physical and institutional foundation for future high-efficiency, large-scale inland water body and flood event monitoring using BeiDou navigation satellite constellations.

5. CONCLUSION AND OUTLOOK

Spaceborne Global Navigation Satellite System-Reflectometry (GNSS-R) technology has undergone a leap-forward evolution from early single-polarization modes (such as single left-hand circular polarization reflection reception) to dual-polarization modes. However, when facing the need to disentangle complex surface environments and deep-layer scattering mechanisms, the information dimension of traditional polarization modes remains inherently limited. The in-depth development of future compact polarimetric technology and the precise reconstruction of full Stokes vectors will provide powerful potential observation means for high-precision, independent monitoring and retrieval of typical land surface hydrological cycles (such as soil moisture, surface freeze-thaw, and inland water body dynamics).

Although the current scientific community has initiated multi-party explorations, existing data sources still have objective limitations in supporting dedicated compact polarimetric GNSS-SAR missions. For instance, the representative commercial small satellite constellations, such as China's "Tianmu-1," mainly acquire multi-polarization reflectivity indirectly through multi-satellite batch configurations of different antenna polarization modes or constellation combinations. In essence, these mostly belong to multi-polarization combinations or "pseudo-compact polarimetric" observations, lacking native, full-path coherent Stokes vector design. As the data source currently most commonly used for compact polarimetric research, SMAP-R was not specifically designed for the compact polarimetric GNSS-SAR mission. Instead, it was obtained through subsequent adaptive adjustment and reconfiguration of the original payload after the failure of its primary radar; therefore, its inter-channel phase noise and hardware isolation are not optimal.

Therefore, how to research, develop, and engineer a "truly compact polarimetric GNSS-SAR" that genuinely adapts to the signal characteristics of the BeiDou Navigation Satellite System (BDS) and possesses native high isolation and broadband coherence will become the core development trend and key breakthrough for the next generation of spaceborne bistatic radar remote sensing. To realize this novel observation approach, specific future implementation pathways mainly include: In the design of antennas and RF front-ends, natively integrating the circular polarization transmit and orthogonal linear polarization coherent receive channels oriented toward the BeiDou signal architecture, thereby guaranteeing high isolation and low crosstalk between channels at the source; breaking through the technical bottlenecks of non-coherent DDM to reconstruct high-fidelity full Stokes matrices; developing daily sliding smoothing and polarization calibration

technologies adapted to the dynamic characteristics of the BeiDou constellation; and in the synergy of physical mechanisms and intelligent retrieval, constructing a physical scattering model and intelligent retrieval framework that integrate full Stokes polarization parameters. This will completely break away from the heavy reliance on external prior auxiliary data, laying a solid foundation for the demonstration and construction of China's independent BeiDou/GNSS-SAR operational satellite constellation.

Declarations

Competing Interests

The authors have no competing interests to declare that are relevant to the content of this article

Compliance with Ethical Standards

Not applicable. This study did not involve human participants, animals, or sensitive personal data.

Author Contribution

X.R.W. conceived the study, designed the methodology, performed formal analysis, acquired funding, provided resources, supervised the work, and wrote, reviewed and edited the manuscript. X.R.W. and S.L.W. carried out investigation. X.R.W. and R.J.S. prepared the original draft. All authors reviewed the manuscript.

Acknowledgments

This work was supported by the National Key Research and Development Program of China

(2024YFB3910000) and the National Natural Science Foundation of China (42061057). The

funders had no role in study design, data collection and analysis, decision to publish, or

preparation of the manuscript.

Data availability statements

Data sets generated during the current study are available from the corresponding author on reasonable request.

References

1. Hall CD, Cordey RA (1988) Multistatic scatterometry, in Proc. IEEE Int. Geosci. Remote Sens. Symp. *(*IGARSS*)*, pp. 561–562
2. Martín-Neira M (1993) A passive reflectometry and interferometry system (PARIS): Application to ocean altimetry. ESA J 17(4):331–355
3. Jin SG, Wu X, Qiu H (2025) GNSS-Reflectometry: Fundamentals, Methods and Applications. Berlin, Germany: Springer
4. Wu X (2025) Research on compact polarimetric GNSS-ReSAR land surface remote sensing technology. Adv Earth Sci 40(9):902–915
5. Unwin MJ, Gleason S, Brennan M (2003) The space GPS reflectometry experiment on the UK disaster monitoring constellation satellite, in Proc. ION GNSS, pp. 2656–2663

6. eoPortal TechDemoSat-1. Accessed: Jan. 4, 2016. [Online]. Available: https://directory.eoportal.org/web/eoportal/satellite-missions/t/techdemosat-1
7. Ruf CS, Gleason S, Jelenak Z et al (2012) The CYGNSS nanosatellite constellation hurricane mission, in Proc. IEEE Int. Geosci. Remote Sens. Symp. (IGARSS), pp. 214–216
8. Yang G, Bai W, Wang J et al (2022) FY3E GNOS II GNSS reflectometry: Mission review and first results, Remote Sens., vol. 14, no. 4, Art. no. 988. 10.3390/rs14040988
9. Jales P et al (2023) Spire Global's operational GNSS-reflectometry constellation for Earth surface observations, in Proc. IEEE Int. Geosci. Remote Sens. Symp. (IGARSS), Pasadena, CA, USA, pp. 884–887. 10.1109/IGARSS52108.2023.10282940
10. Unwin MJ et al (2021) An introduction to the HydroGNSS GNSS reflectometry remote sensing mission. IEEE J Sel Top Appl Earth Observ Remote Sens 14:6987–6999. 10.1109/JSTARS.2021.3089550
11. Raney RK (2007) Hybrid-polarity SAR architecture, IEEE Trans. Geosci. Remote Sens., vol. 45, no. 11, pp. 3397–3404, Nov. 10.1109/TGRS.2007.895883
12. Huang F et al (2025) Tianmu-1 constellation GNSS-R in-orbit performance: Spatiotemporal characteristics, product applications, and polarimetric features, IEEE Trans. Geosci. Remote Sens., vol. 63, Art. no. 5802020. 10.1109/TGRS.2025.3581343
13. Charbonneau FJ, Brisco B, Raney RK et al (2010) Compact polarimetry overview and applications assessment. Can J Remote Sens 36:S298–S315. 10.5589/m10-062
14. Souyris JC, Imbo P, Fjortoft R et al (2005) Compact polarimetry based on symmetry properties of geophysical media: The π/4 mode, IEEE Trans. Geosci. Remote Sens., vol. 43, no. 3, pp. 634–646, Mar. 10.1109/TGRS.2004.842486
15. Hagfors T, Brockelman RA, Danforth HH, Hanson LB, Hyde GM (1965) Tenuous surface layer on the Moon: Evidence derived from radar observations, Science, vol. 150, no. 3700, pp. 1153–1156, Nov
16. Munoz-Martin JF, Rodriguez-Alvarez N, Bosch-Lluis X, Oudrhiri K (2022) Stokes parameters retrieval and calibration of hybrid compact polarimetric GNSS-R signals, IEEE Trans. Geosci. Remote Sens., vol. 60, Art. no. 5113911. 10.1109/TGRS.2022.3178578

Figures

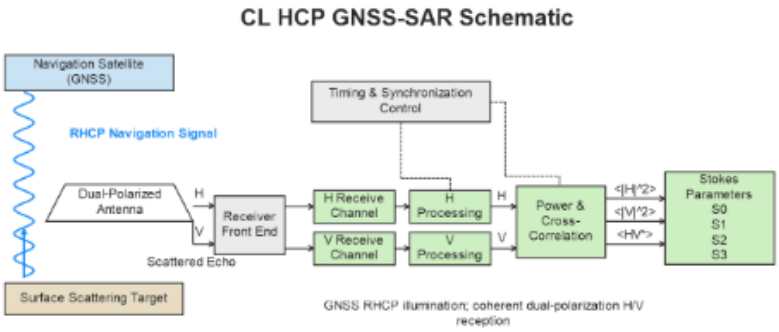

Figure 1

System architecture and signal processing flowchart of the circular-linear compact polarimetric GNSS-SAR [11]

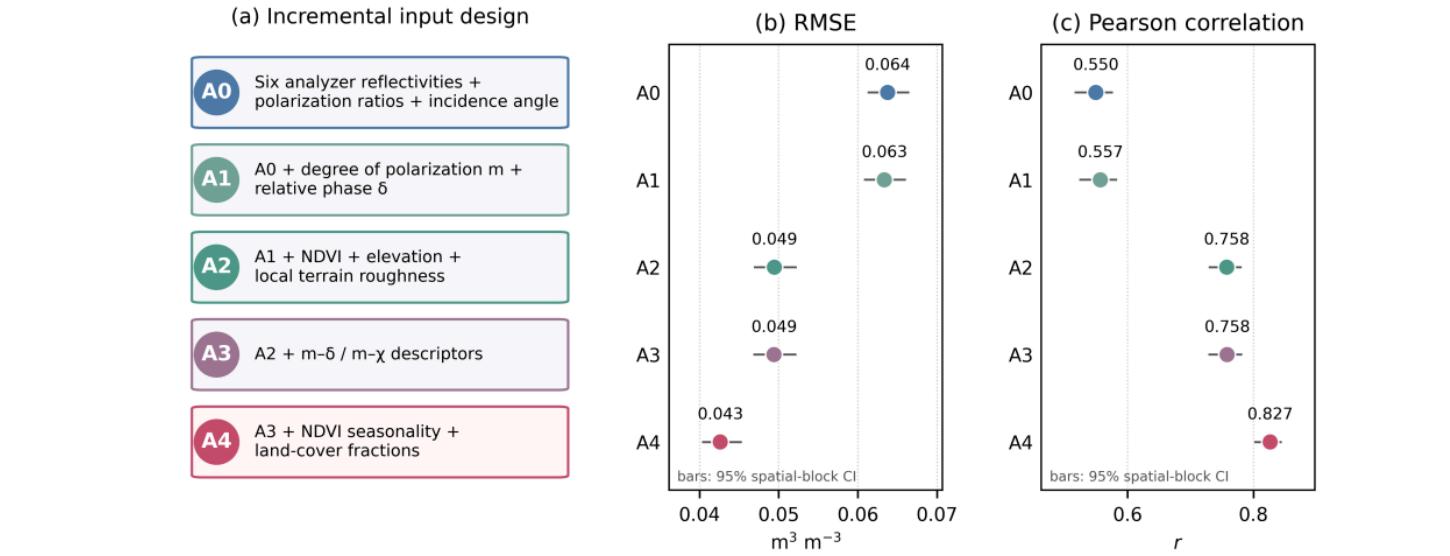

Figure 2

SMAP-R soil-moistrue retrieval with polarimetric and auxiliary information

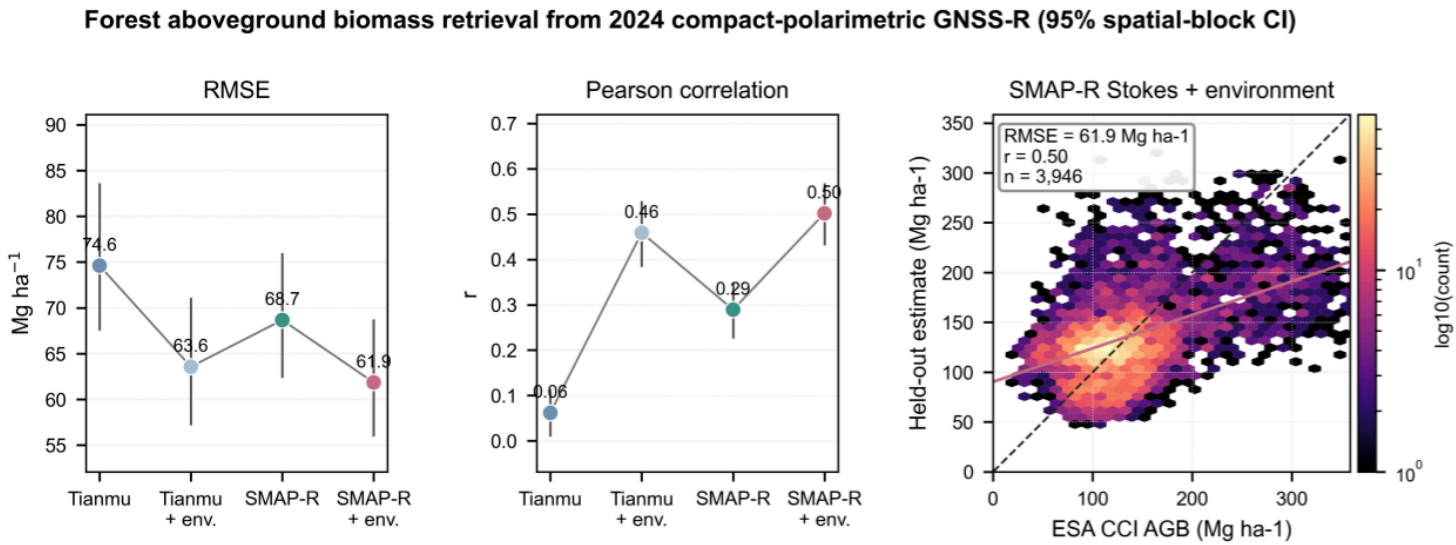

Figure 3

Model performance evaluation and scatter density comparison (95% spatial block confidence intervals) for Forest Aboveground Biomass (AGB) retrieval based on 2024 compact polarimetric GNSS-R observations: (a) Root Mean Square Error (RMSE) of four feature configuration schemes (Tianmu-1, Tianmu-1 + environmental auxiliary variables, SMAP-R Stokes, SMAP-R Stokes + environmental auxiliary variables); (b) the corresponding Pearson correlation coefficient ( ); (c) Scatter density comparison between the predicted values of the optimal model (SMAP-R Stokes + environmental variables) and the ESA CCI AGB reference data ( ). The error bars in panels (a) and (b) represent the 95% confidence intervals obtained from a 300 spatial block Bootstrap resampling calculation.

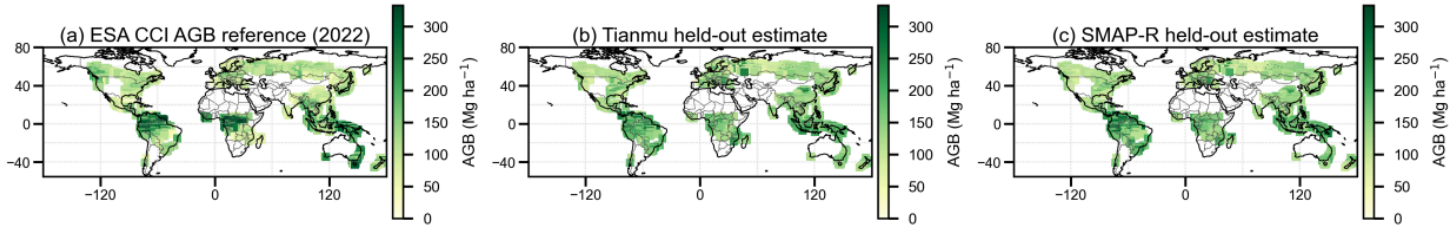

Figure 4

Comparison of global forest Aboveground Biomass (AGB) retrieval results at 36 km spatial resolution based on a common forest support mask: (a) ESA CCI AGB reference benchmark product (2022); (b) Tianmu-1 spatial hold-out cross-validation retrieval results; (c) SMAP-R spatial hold-out cross-validation retrieval results. All maps utilize the identical valid forest mask, and the biomass density unit is Mg ha^{-1}.

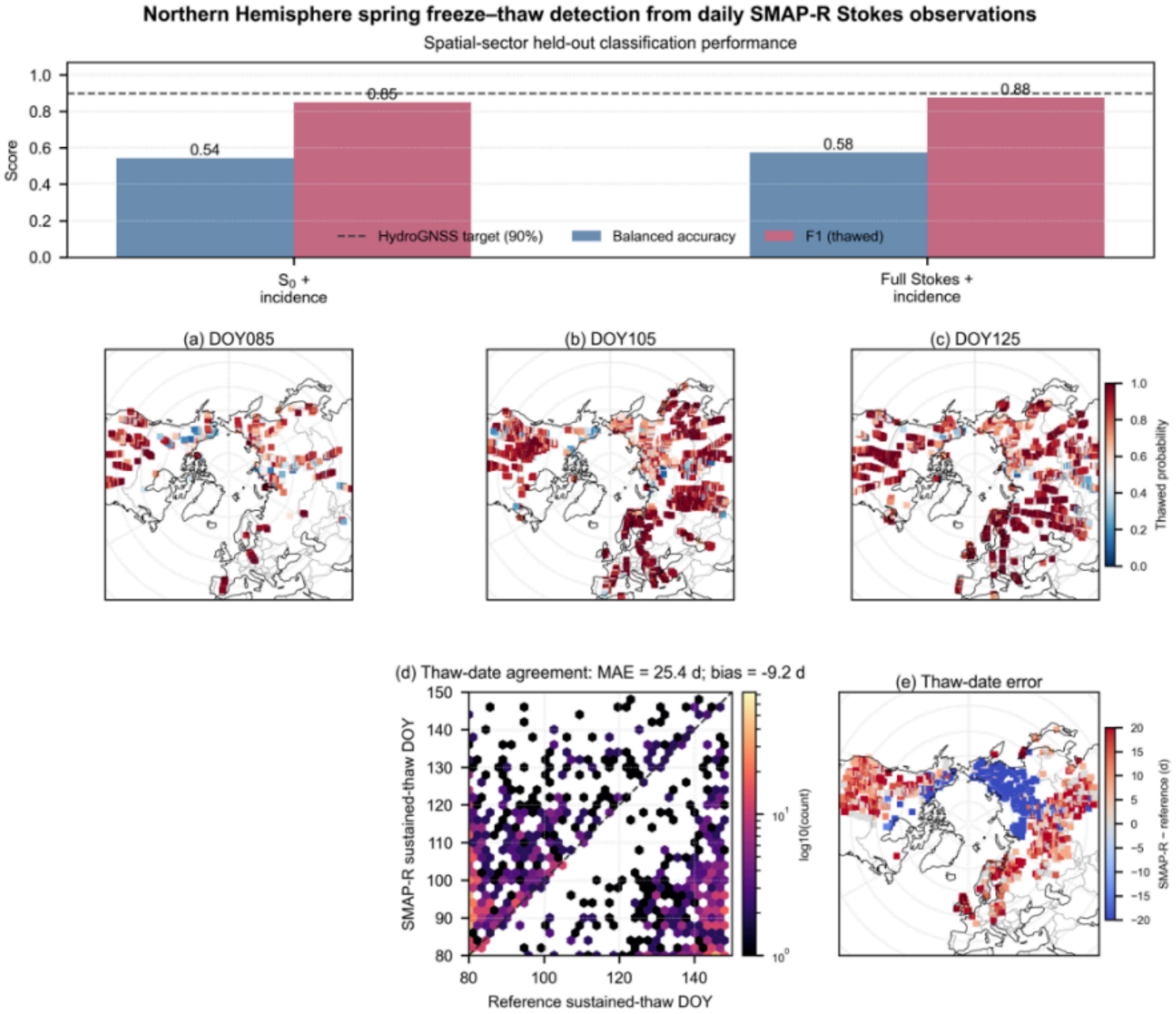

Figure 5

Detection Performance and Spatiotemporal Dynamics of Northern Hemisphere Spring Surface Freeze-Thaw States Based on Daily-Scale SMAP-R Stokes Observations (DOY 080–179, 2024). (a–c) Spatial distribution of thaw probabilities at typical moments in the Northern Hemisphere under spatial block hold-out cross-validation: (a) DOY 085, (b) DOY 105, (c) DOY 125; (d) Scatter density comparison and statistical metrics between the continuous thaw onset day (DOY) identified by SMAP-R and the reference continuous thaw day; (e) Spatial distribution map of thaw date error (SMAP-R estimated value minus reference value). The top bar chart compares the performance of the baseline feature (S_0 + incidence angle) and the full Stokes feature (Full Stokes + incidence angle) in terms of balanced accuracy and thaw-class F_1-score.

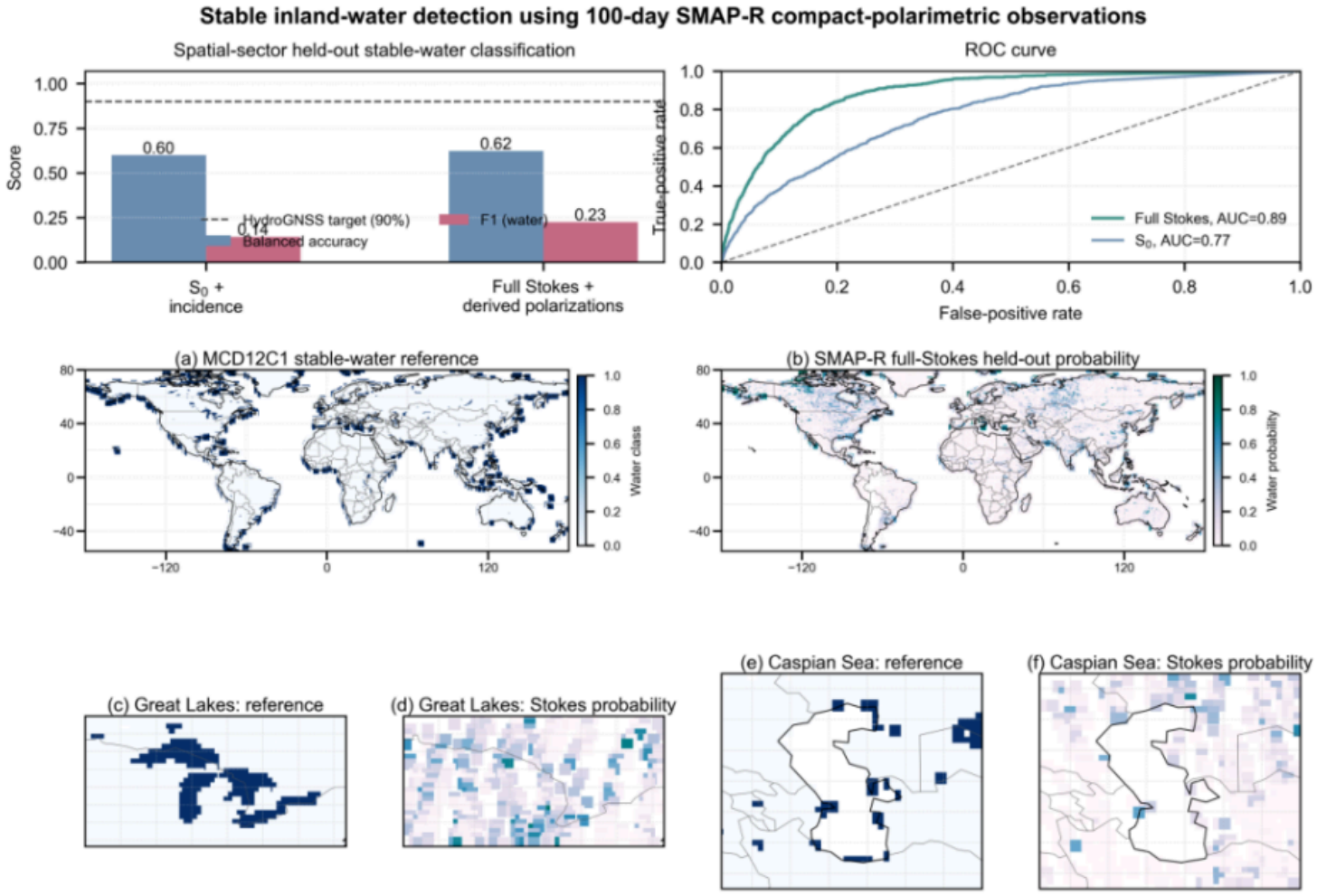

Figure 6

Comparison of Stable Inland Water Body Spatial Identification Performance Based on 100-day SMAP-R Compact Polarimetric Observations

(a) Bar chart comparing the classification performance of stable water bodies under spatial sector hold-out cross-validation (including balanced accuracy and water body F_1-score; the dashed line indicates the HydroGNSS 90% task design target); (b) The corresponding Receiver Operating Characteristic (ROC) curve and AUC performance of the feature schemes; (c) Global stable water body reference benchmark based on MCD12C1 aggregated to 36 km; (d) Spatial hold-out water body prediction probability field of SMAP-R full Stokes features; (e, f) Local comparison of reference values and SMAP-R prediction probabilities in the Great Lakes and Caspian Sea regions. The data are constructed based on 100-day cumulative observations during the period of DOY 080–179, 2024.